International Conference on Advances in Materials, Computing and Communication Technologies
In Association with International Journal of Scientific Research in Science and Technology
Volume 9 | Issue 1 | Print ISSN: 2395-6011 | Online ISSN: 2395-602X (www.ijsrst.com)

Investigation on Microstructure And Mechanical Characterization of Tig Welded Inconel 625 Nickel Based Alloy

M. Ajith Kumar*[1], M. Vinoth Pandiyan[2], P. Krishnan[2], S. Rajiv[2]
[1]Assistant Professor /Mechanical Department/Mangayarkarasi College of Engineering, paravai, Madurai, Tamil Nadu, India
[2]UG Students/Mechanical Department/Mangayarkarasi College of Engineering,paravai ,Madurai, Tamil Nadu, India

ABSTRACT

This paper deals with joining of 4 mm thick plates of Inconel 625 and ferritic stain- less steel (S.S) 316L by Tungsten Inert Gas (TIG) welding process without using the activated flux. Trial experiments were conducted to find the influence of welding current on the depth of penetration and depth to width (D/W) ratio. The studies proved that a complete penetration could be achieved in multi pass. Microstructure examination using optical and Scanning Electron Microscope (SEM) clearly exposed the development of unmixed zone and also the Heat Affected Zone (HAZ) of Inconel 625. The chemical components of the Inconel 625 and SS316L were determined using Energy Dispersive Analysis (EDAX). Tensile and bend failures were observed at the parent metal of Inconel 625 , SS316L and Inconel 625 & SS316L dissimilar joints. It was indicated from the notch tensile studies that the notch strength ratio was better than unity, which established that the weldments were ductile in all circumstances. The corrosion studies were carried out in the Nacl solution and it was found that Inconel 625 and SS316L dissimilar joint possess less corrosion resistance than similar SS316L weldment. It was inferred from the current study that the ultimate tensile strength of dissimilar weldments was better compared to similar weld-ments and the failure was observed in the parent metal for all the cases. Bend test results portrayed that dissimilar weldments possess better strength compared to SS316L weldments.

Keywords : Inconel625 @ SS 316L, TIG welding Mechanical properties Corrosion behaviour

I. INTRODUCTION

Inconel is a registered trademark of Special Metals Corporation for a family of austenitic **nickel-chromium-based super alloys.** [1]

Inconel alloys are oxidation-corrosion-resistant materials well suited for service in extreme environments subjected to pressure and heat. When heated, Inconel forms a thick, stable, passivating oxide layer protecting the surface from further attack. Inconel retains strength over a wide temperature range, attractive for high temperature applications where aluminum and steel would succumb to creep as a result of thermally induced crystal vacancies. Inconel's high temperature strength is developed by

solid solution strengthening or precipitation hardening, depending on the alloy.

II. PROBLEM IDENTIFICATION

From the literature review, it is found that welding of inconel 625 Nickel based Alloy is a big challenge by conventional arc welding process. Again repeatability of welding depends on its control on welding speed and other Comparison of various mechanical properties between the inconel 625 and stainless steel 316L analyzed. To get better strength welding of the Inconel 625 Alloy plate also done from both side. Effect of welding speed and applied current on the tensile strength of weld joint, micro hardness of the weld pool and macrostructure of the joint was analyzed.

III. METHODS AND MATERIAL

PRE WELDING PROCESS

Thermal (heat) treatment is any application of a temperature, for any amount of time, sufficiently high enough as to accomplish one of the following: (1) reduce stresses, (2) allow atom movements to redistribute existing alloy elements, (3) promote grain growth, (4) promote new recrystallization, (5) dissolve phases, (6) produce new phases owing to precipitation from solid-solutioning, or (7) support alloy surface chemistry. Prior to welding, the following thermal treatment was performed in order to place the base material in a fully solutioned (weldable) condition and to obtain complete recrystallization and maximum softness. The pre-weld solution was performed in an vacuum atmosphere where (1) the base material specimens were heated to a temperature of 1750°F ± 25°F and held for a period of 60 minutes, then (2) cool to a temperature of 1100°F at a rate of 35°F/minute proceeded by (3) continued cooling to a temperature of 1000°F at a rate of 15°F /minute; all remaining subsequent cooling rates were 1750°F/minute. All cooling procedures were produced via back-filling with 100% argon gas. After welding, the following solution thermal treatment was performed to resolve any residual stresses and dissolve any secondary phases and prepare the alloy for subsequent aging. The aging is performed to obtain maximum ductility, this process also homogenizes the microstructure prior to aging.

Like the initial solutioning treatment, the weldment specimens were once again (1) heated to a temperature of 1750°F ± 25°F and held for a period of 60 minutes, then (2) cooled to a temperature of 1100°F at a rate of 35°F/minute and proceeded by (3) continued cooling to a temperature of 1000°F at a rate of 15°F /minute; all remaining subsequent cooling rates were 50°F/minute and cooling procedures were produced via back-filling with 100% argon gas. Immediately following the solution treatment, the weldment specimens were placed through the following precipitation (aging) thermal treatment to bring out the desirable strengthening precipitates and control other secondary phases, including carbides and detrimental topographically close packed phases. Some of the topographically close pack phases include σ, μ, and Laves which are variably detrimental when more than trace amounts are present. The weldment specimens were (1) heated to a temperature of 1325°F ±25°F and held for a period of eight hours, then (2) cooled at a rate of 100°F ±25°F/hour to a temperature of 1150°F ±25°F and again held for a period of 18 hours; all remaining subsequent cooling rates were 50°F/minute and all cooling procedures were produced via back-filling with 100% argon gas.

CHEMICAL COMPOSITION

INCONEL alloy 625 is readily joined by conventional welding processes and procedures. INCONEL Filler Metal 625 and INCONEL Welding Electrode 112 are nickel-chromium-molybdenum products designed for welding INCONEL alloy 625

to itself and to other materials. Compositions of the two products are shown in Table 13. Like alloy 625, deposited weld metals from both products are highly resistant to corrosion and oxidation and have high strength and toughness from the cryogenic range to 1800°F. They require no postweld heat treatments to maintain their high strength and ductility. When used to weld INCONEL alloy 625 to dissimilar metals, both products tolerate a high degree of dilution yet maintain characteristic properties.

INCONEL Filler Metal 625 and INCONEL Welding Electrode 112 are also used as "over-matching composition" welding products for iron-nickel-chromium-molybdenum corrosion-resistant alloys including 316 and 317 stainless steels, 6% molybdenum super-austenitic stainless steels, INCOLOY® alloys 825 and 020, and INCONEL alloy G-3. The higher alloy content of the alloy 625 welding products offsets the effects of elemental segregation in weldments which can result in preferential weld corrosion

INCONEL Filler Metal 625 is designed for use with the gas tungsten-arc and various gas-metal-arc processes. Operating characteristics are similar to those of other nickel-chromium filler metals. INCONEL Welding Electrode 112, for shielded metal-arc welding, has excellent operability. The slag produced is hard, but it detaches in large sections when fractured, leaving clean weld metal.

[a] Deposited weld metal. [b] Plus cobalt. [c] When specified.

The as-received nickel-based superalloy Inconel 625 plate with 6.5 mm thickness was cut to 50 mm 9 50 mm 9 6.5 mm dimensions using wire cut electrical discharge machining. The chemical composition of the base metal was confirmed using an optical emission spectrophotometer (OES) with the corresponding weight percentages being shown in Table 1. For bead on trial welding, Inconel 625 plates were machined to coupons of 300 mm 9 150 mm 9 6.5 mm size for A-TIG welding. The machined

Several weldments with varying parameters were prepared in order to meet the parameter optimization, heat treatment, metallographic review and NDE (Ultrasonic test , X-ray and FPI), objectives of this research. Each weldment represents the various weld profiles and geometries. These geometries include straight single-line beads, straight-line-weave pattern beads, circular weld build-ups techniques - Ultrasonic test, X-ray and FPI - to ensure weld quality (e.g. porosity, lack of fusion, and cracking, and material edge build-ups which are representative of the most common weld styles in aerospace applications. All specimens were heat treated accordingly, with a pre- and post-weld solution heat treatment and finally an age treatment. All weldments were then macro-evaluated using common NDE).

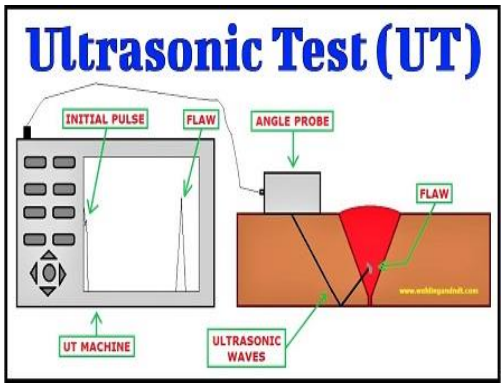

Fig 1. Schematic diagram of the ultrasonic Test

WELDMENT SPECIMEN FABRICATION:

1. Base metals and welding process

The base metal considered in the study of Inconel 625 and SS 316 L thick plates were purchased from Metline Industries Ltd., Mumbai. The microstructure of the base metals was obtained, using optical microscopy as shown in Fig. 61. The presence of Ni rich austenitic matrix and Nb. Ti rich phases in the form of precipitates were also perceived in Inconel 625 boundaries. The as-received plates of Inconel 625 and SS 316 L were

machined to rectangular samples of dimensions 150 mm x 50 mm x 5 mm using wire-cut electrical discharge machining (WEDM). These samples were first acid preserved to remove any filth, burs etc. Before welding, standard V-Butt configurations were employed on the samples. Based on the review (2, 5 & 7), the optimum weld process parameters employed in this study is listed in Table 1. High purity argon gas was used as shielding gas, with a flow rate of 15 L per minute. The diameter of the filler wire considered in this study was 1.5 mm, the electrode tip angle was 60° at a constant welding

Process parameters for TIG-welding of Inconel 625 and SS 316L weldments.

Process Parameter	Values
Voltage	12 V
Current	120 A
Electrode diameter	1.5 mm
Electrode tip angle	60°
Shielding gas	Argon
Flow Rate	15 L
Welding speed	80 mm/min

Speed of 80 mm/min. After welding, the weldments were machined to different coupons of various dimensions according to ASTM E3 standards for carrying out the metallurgical, mechanical tests to establish the structure- property relationship for these weldments. Further, the weldments were exposed to a corrosive environment consisting of the Nacl solution at room temperature. The proce- dure involved in the metallurgical, mechanical tests and corrosion studies are explained in the sub-sequent sections.

Metallurgical and mechanical characterization

Microstructure investigation of the weldments was carried out on machined (Perpendicular to the welding direction) coupons of dimensions 25 mm x 10 mm x 4 mm which covered all the compos- ite zones such as Parent metals, HAZ & Weld zone. The surface of the coupons was prepared to get mirror like finishing using typical metallographic procedures such as mechanical and disc polishing were engaged because SS316L and Inconel 625 are relatively easy to polish. Electrolytic etching was used to expose the microstructures at various zones of the weldments. It is similar to chemical etching, in which acids and bases are used for modifying the pH. However, the electrochemical potential is controlled electrically by varying either the voltage or current externally. Electrolytic etching is often used for harder-to-etch specimens that do not respond well to basic chemical etching techniques. Both Optical Microscope (OM) and Scanning Electron Microscope (SEM) techniques were engaged to examine the microstructure changes on the weldments. Tensile and bend test were conducted on the fabricated weld- ment as per the ASTM: E8/8M and ASTM: E190-92 standards, using Instron Universal Testing Machine. Microhardness measurements were also taken on the weldments, using Vicker's microhardness tester. The hardness computations were done at steady intervals across the entire width of the dissimilar weldments in order to estimate the precise changes. A load of 500 gf and a dwell time of 15 s were employed to compute the hardness deviations of the weldments.

Corrosion behaviour

Corrosion studies were performed on the weldments of dimen- sions 10 mm x 10 mm x 4 mm and on the composite zones of the dissimilar weldments using WEDM. Mirror polished surfaces were prepared before

conducting the corrosion experiment. The test samples were exposed to 3.5 wt.% Nacl solution with pH value of 6.5–7.25 [15]. Weight losses were taken at the end of every cycle, using digital weighing balance with a sensitivity of 0.01 mg. The above procedure was repeated for five samples and the average results weretaken. Weight measurements were taken for 24 h, 48 h, 72 h, 96 h and 120 h respectively

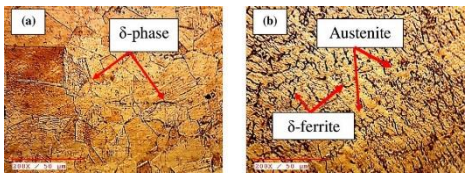

Fig 2. Microstructure of the base metal (a) Inconel 625 and (b) SS 316L.

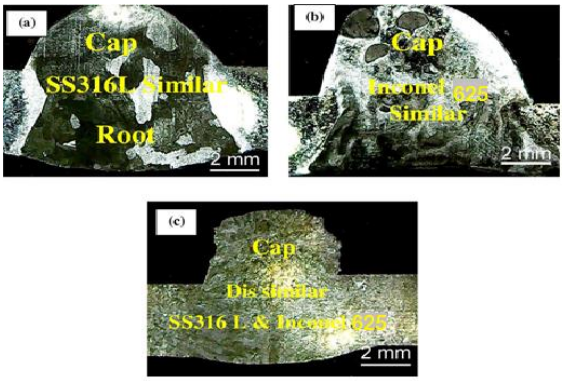

Fig 3. Cross section macro-photographs of weldments (a) SS316L similar joints (b) Inconel 625 similar joints (C) SS316L and Inconel 625 dissimilar joints.

IV. RESULTS AND DISCUSSION

***Macrostructure investigation**

The cross-section macrographs of the welded coupons are shown in Fig 39(a–c). All the filler metals have shown better results in terms of fusion with the base metals [13].

***Metallurgical examination of the weldments**

Interface microstructures of the weldments are shown in Fig. 60(a–c). A prominent unmixed zone was seeming at the HAZ of Inconel 625. The appearance of unmixed zone could be endorsed as a result of multi pass welding and also due to the use of over alloyed filler metals. In dissimilar welding, an unmixed zone is often perceived when the melting range of the filler materials is superior to that of the melting range of the base materials. From the 3g. 3 (a–c), it is inferred that the formation of secondary phases was observed at the heat affected zone (HAZ) of both the weldments. However, the dispersal of secondary phases as well as the width of HAZ was found to be insignificant as compared to the earlier studies of various researchers [10–12]. Weld microstructure showed the presence of tiny precipitates at the inter-dendritic regions of both the weld and fusion zones, which was also ascertained from the OM analysis as black phases [13,14].

*Fig. 61(a–b) shows the SEM micrograph of weldments. Fig. 61 reveals the grain boundaries, witnessed at the HAZ of Inconel 625. EDAX analysis [Fig 39(a–b)] was carried out across the parent metal to HAZ of dissimilar joints showed that the Nb, Cr and Ni rich phases were present at the HAZ and found to be more than the parent metal. Similar precipitation was observed within the HAZ of Inconel 625 in the case of weldment too. Furthermore, there was no liquid cracking noticed at the HAZ of Inconel 625, which clearly shows the absence of delta phases. Moreover, these elements were exhausted in the matrix of the fusion zones. The retention of Nb in the austenite was much lower due to their large radii associated to other elements in the weld zone which resulted in isolation. Even though the existence of Nb was perceived in the fusion zones of both the weldments, this could be attributed to the element movement exclusively Nb from either of the parent metals to the fusion zone.

Microstructures at the fusion zone exhibited the presence of fine equiaxed dendrites at the root passes and additionally on the cen- tre of the fusion zone of the weldments. In general, the formation of fusion zone microstructure is influenced in many ways by cur- rent pulsing [11]. In distinction to the traditional constant current methodology, the solidification process is sporadically interrupted.

. SEM micrograph of dissimilar weldments (a) Weld interface (b) Fusion zone.

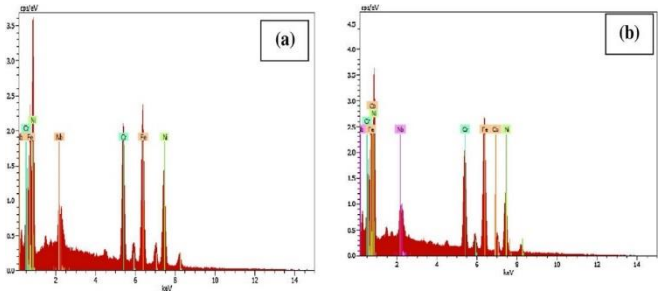

Fig 4. (a) EDAX analysis of dissimilar joints (b) EDAX analysis of dissimilar joints in heat affected zone.

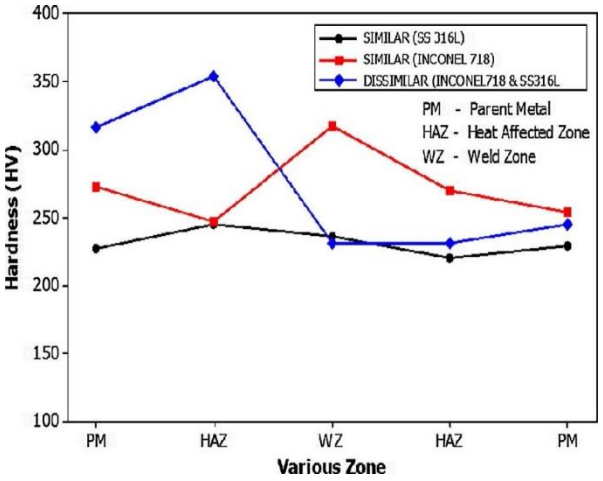

Fig 5. Hardness profile of the different weldments.

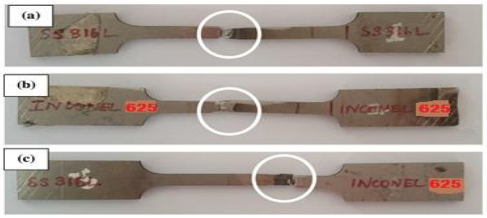

Fig 6. Tensile fracture photograph of the weldments (a) SS316L similar joints (b) Inconel 625 similar joints (C) SS316L and Inconel 625 dissimilar joints.

By the flow of two different currents, specifically peak current and background current. Owing to these currents, there exists a cyclic eccentricities of energy input into the weld pool that consecutively causes thermal fluctuations. The pulsed peak current deteriorates the solid-liquid interface and advances towards the arc, making it progressively susceptible to any interludes within the arc form. When the current is again accrued within the subsequent pulse, the grain growth is detained and re-melting of the growing dendrites occur. In addition to that, the current pulsing resulted within the periodic fluctuations of the arc forces and therefore fur- ther fluid flows, which might tend to lower temperatures ahead of the solidifying interface. Moreover, the temperature fluctuations which are essential in pulsed welding leads to a continual amend- ment within the weld pool size and shape favoring the expansion of new grains [14]. It's inferred that due to the reheating and re-melting actions experienced throughout the multi-pass welding, the grains were recrystallized at the root pass of the weldments. Furthermore, as the direction of maximum thermal gradient at the solid-liquid interface changes continuously, the newer grains fre- quently become favorably oriented. However, each columnar and equiaxed grain growth was ascertained on the edges of the fusion zone in both the cap and filling passes of the fusion zones. SEM micrographs inferred the presence of micro segregates in both the fusion zones of

dissimilar weldments. It's ascertained from the EDAX analysis that these micro-segregates were enriched in Nb, Ni and Cr for the weldments. Additionally, these elements were depleted within the matrix of the fusion zones. These micro- segregates weren't found to be Laves phase as determined from the EDAX compositional analysis.

5.1.2Mechanical characterization

Hardness contours of the dissimilar weldments concerning SS316L and Inconel 625 employed are shown in Fig. 60 and the hard- ness data points of the weldments are shown in Table 2. It is inferred from the contours that the hardness values at the fusion zones of the weldments are established slightly greater than Inconel 625. There were not much difference observed in the hardness val- ues at the fusion zone of other similar weldments. This could be attributed to the similar chemical composition of the fillers except for some insignificant differences in the elements such as Nb, Ni and Cr etc. A closer investigation revealed that the root region of hardness of points

*The dissimilar weldments experienced higher hardness values as compared to other regions. The average hardness at the root pass of the weldments were found to be 350 HV. As explained in the pre- vious section, the root region undergoes re-heating and re-melting actions due to multi-pass welding which would result in the den- drite fragmentation and the formation of finer equiaxed dendrites [14]. The grain improvement experienced due to current pulsing could be coherent for the higher hardness in the fusion zone. The higher attentiveness of Nb in the fusion zone also increases the hardness, due to the distortion developed in the matrix by this ele- ment owing to its large radii. Likewise, the presence of elements such as Cr to Ni in these fillers could also be accredited to the greater hardness values in the fusion zones.

The tensile test outcomes exhibited that a fracture occured at the parent metal or well away from the fusion zone for the weld-ments in all the trials. It reveals that the joint strength were higher than that of the parent metal. Fig. 61 shows the tensile test sam-ples with the fracture experimented conditions. The typical tensile stress-strain curves obtained at room temperature is shown in Fig 39. During the transverse tensile tests, all weldments failed at the weaker parent metal. Inconel 625 base metal has a natu- rally coarse and fully dendritic microstructure, which leads to low impact toughness and ductility. Thus, the metal failed before expe- riencing a remarkable amount of plastic elongation. The typical tensile strength of dissimilar joints was found to be 632 Mpa (Fig 39). It is obvious from the tensile micrographs (Fig. 60(a–c)) that both

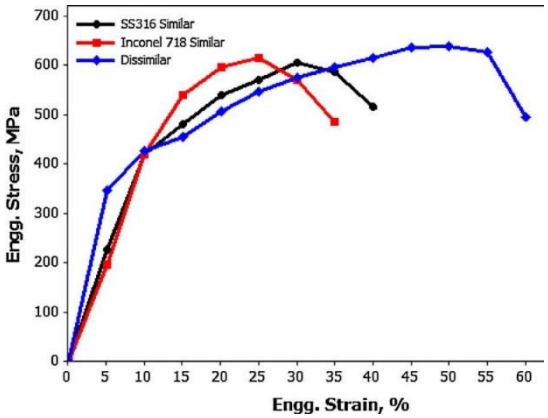

Fig 7. Tensile result of the weldments.

the weldments undergo severe plastic deformation and exhibit the enhanced strength and ductility. The enhanced strength of the as- welded Inconel 625 dissimilar weldments could be attributed to the occurrence of minimal amount of laves

phase in fusion zone [19]. SEM fractographs (Fig. 60(a–c)) shows the presence of dimples and voids as the fracture topology of the weldments. Neverthe- less, there was numerous discontinuous bands of secondary phase

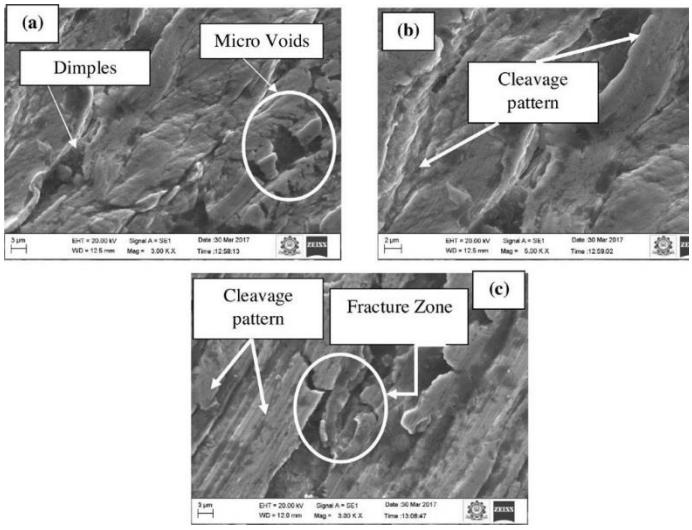

Fig 8. SEM micrograph of the fracture zone (a) SS316L similar joints (b) Inconel 625 similar joints (c) SS316L and Inconel 625 dissimilar joints.

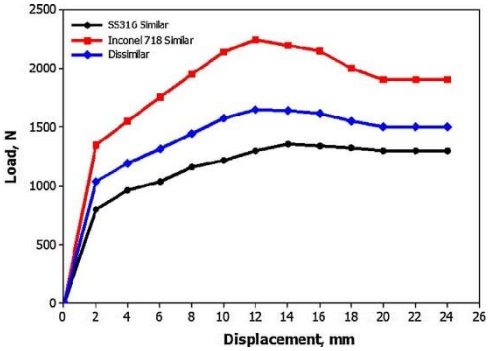

Fig 9. Bend test results of the weldments.

Perceived in the SEM morphology. Microstructure of Inconel 625 is composed of dendrites that endorse the brittle fracture. In contrast, SS316 base metal has greater toughness that can be attributed to the presence of wrought and austenitic grains. Fracture surface of this base metal is composed of deep and wide dimples, which illustrate the higher resistance of dissimilar weldment to fracture. Occur- rence of laves phase affords favorable sites for stress-free crack initiation and propagation in the dissimilar weldments. On the other hand, the weld metal displays fully ductile fracture, except Inconel 625, exhibits mixed fracture mode. It can be seen that the fracture surface is composed of regions of cleavage fracture and plastic deformation.

Bend test of the parent metals and the dissimilar weldments was conducted at room temperature condition. Both the weldments underwent deformation without complete rupture. Fig. 610 illus- trates the bend test results of the weldments. Fig. 610 reveals that dissimilar weldments experienced enhanced toughness compared to the SS316L parent material. However, the bend toughness of both the weldments were slightly lower than that of the base metals hired in the study. The improvement in the values could be ascribed to the higher Nb content in the inter-dendritic regions of the fusion zones. Moreover, the existence of secondary phases or segregates with the elements Nb, Ni and Cr located at inter-dendritic regions that formed as terminal solidification products, have a detrimental effect on the toughness of the fusion zone. Upon loading, both the weldments underwent complete fracture by perceiving a complete breakage as shown in Fig. 611(a–c). Failure analysis was conducted on the specimens after the bend test. Fig. 611(a) shows the loca- tions of SEM observations on the failure surface of a specimen. It is observed in Fig. 611(b–c) that the crack propagates through the weld region. The crack bowing around the particles or interfacial failure are not observed in these micrographs. It is also observed that the weldments develop numerous other cracks as well, which is likely due to the difference in failure strain of the particle material and the matrix material. In some cases, the crack may

be slightly offset because of the localized structure of the weldments [21–26]. The lower value of toughness could be attributed to the existence of inclusions caused by the oxide in the weld metal. Similar results have been published elsewhere [16–20]. In addition to that, the hardness of the fusion zone was slightly higher than that of the parent metals due to the enhancement of various strengthening elements in the fillers active in the study [13,14]. Further, SEM fractographs of the bend tested dissimilar weldments also revealed the presence of cracked boundaries with the discrete, continuous splats running on the matrix which indicate a mixed mode of fracture experienced during impact loading.

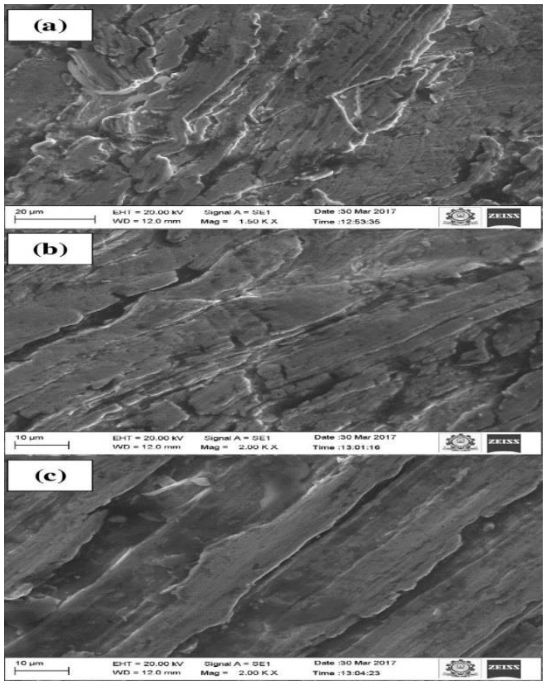

Fig 10. Fracture zone of weldments (a) SS316L similar joints (b) Inconel 625 similar joints (c) SS316L and Inconel 625 dissimilar joints.

5.2.1Corrosion behavior

Estimation of the performance of the weldments in service con- ditions was made by exposing the weldments into a Nacl solution at room temperature. Table 3 shows the various stages of corroded samples of SS316L Similar, Inconel Similar and dissimilar weld- ments exposed in Nacl bath. It was found that some local regions of weld joint suffered slight local corrosion attack, but the corrosion of base zone (BZ) was not apparent. Small precipitated phases were formed in the weld joint during the weld process. At the same time, the small defects such as pores are easily attacked by the aggressive solution and increases the corrosion susceptibility of some localized regions in the weld joint [15].After 24 h (1st day), the weldments were stained to bluish colour; the parent metal Inconel 625 changed to greyish colour, Micrographs of corroded samples exposed in Nacl bath.

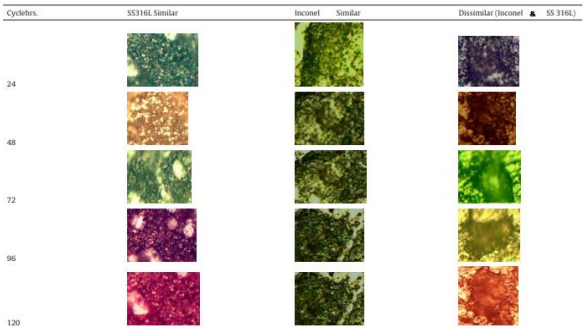

Fig 11. Corrosion plot for working hr vs weight loss for similar and dissimilar weldments in Nacl solution.

Whereas SS 316L did not show any deviations in its colour. After 48 h (2st day), scales were formed on Inconel 625 and got intensified during the progression of corrosion cycle which led to spallation of the oxide scales starting from middle of the cycles and continued till 120 h. The colour of the scale transformed from brownish to black during the corrosion cycle for Inconel 625. The fusion zones weldments exhibited a substantial weight loss and there was swel- tering and spalling of the scales. Pale greenish traces were observed at 72 h and yellowish spots were formed at 96 h which seemed till

the 120 h. Spallation was detected in both fusion zones and in the parent metal, Inconel 625, which intensified from corrosion cycle with the scales spalling in the boat. The surface of these coupons became coarser with progressive acquaintance of time, and uni- form pitting was perceived throughout the surface of the samples [15]. It is also inferred that there was no spallation detected on the parent metal to Inconel 625 from the beginning to the end of the corrosion cycle. Fig. 612 shows that the weight deviations are con- tinuous in all the coupons while exposing to the room temperature. The weight deviations at the end of corrosion were calculated to be 0.0191 g, 0.0114 g and 0.0492 g for the Inconel 625 similar, SS 316L similar and dissimilar joints respectively

V. CONCLUSION

This study addresses the successful joining of SS 316L similar, Inconel 625 Similar and SS316L & Inconel 625 dissimilar weldments using TIG welding. The following are the outcomes drawn from the present study.

- ✓ Successful joints of similar and dissimilar joints could be achieved by TIG welding. There was no solidification or HAZ liquid cracking during the multi-pass welding of these joints.
- ✓ Microstructure studies revealed the formation of HAZ and
- ✓ Unmixed zone adjacent to the weld interface of the joints.
- ✓ Laves phase was totally controlled in the weld zone which con- tribute to the improvement of the mechanical properties.
- ✓ Dissimilar weldments possess higher hardness value, whereas other weldments displayed the lowest value among the weld metal investigated. Cr and Ni precipitation in the heat-affected zone of dissimilar weldments occurred.
- ✓ The microstructure showed that the heat-affected zone with inclusions has an impact on the tensile strength.
- ✓ Tensile studies revealed that the fracture was experienced in the parent metal of SS316L. It is proven that the weld strength of both the weldments were better to that of the parent metals.
- ✓ Bend test illustrates that the dissimilar joints have higher strength over the SS316L parent material.
- ✓ Corrosion studies confirmed that the weight loss was found to be minimum in SS316L, than the other weldments

IV. REFERENCES

[1]. en.wikipedia.org/wiki/GTAW
[2]. www.weldwell.co.nz/site/weldwell
[3]. http://www.azom.com/article.aspx?ArticleID=1446
[4]. www.micomm.co.za/portfolio/alfa
[5]. Kumar, S.(2010) Experimental investigation on pulsed TIG welding of aluminium plate. Advanced Engineering Technology.1(2), 200-211
[6]. Indira Rani, M., & Marpu, R. N.(2012). Effect of Pulsed Current Tig Welding Parameters on Mechanical Properties of J-Joint Strength of Aa6351. The International Journal of Engineering And Science (IJES),1(1), 1-5.
[7]. Hussain, A. K., Lateef, A., Javed, M., & Pramesh, T. (2010). Influence of Welding Speed on Tensile Strength of Welded Joint in TIG Welding Process. International Journal of Applied Engineering Research, Dindigul, 1(3), 518-527.

[8]. Tseng, K. H., & Hsu, C. Y. (2011). Performance of activated TIG process in austenitic stainless steel welds. Journal of Materials Processing Technology, 211(3), 503-512.

[9]. Narang, H. K., Singh, U. P., Mahapatra, M. M., & Jha, P. K. (2011). Prediction of the weld pool geometry of TIG arc welding by using fuzzy logic controller. International Journal of Engineering, Science and Technology, 3(9), 77-85.

[10]. Karunakaran, N. (2012). Effect of Pulsed Current on Temperature Distribution, Weld Bead Profiles and Characteristics of GTA Welded Stainless Steel Joints. International Journal of Engineering and Technology, 2(12).

[11]. Raveendra, A., & Kumar, B. R.(2013). Experimental study on Pulsed and Non- Pulsed Current TIG Welding of Stainless Steel sheet (SS304). International Journal of Innovative Research in Science, Engineering and Technology, 2(6)

[12]. Sakthivel, T., Vasudevan, M., Laha, K., Parameswaran, P., Chandravathi, K. S., Mathew, M. D., & Bhaduri, A. K. (2011). Comparison of creep rupture behaviour of type 316L (N) austenitic stainless steel joints welded by TIG and activated TIG welding processes. Materials Science and Engineering: A, 528(22), 6971-6980.

[13]. Yuri,T., Ogata, T.,Saito.M.,& Hirayama,Y.(2000). Effect of welding structure and δ- ferrite on fatigue properties for TIG welded austenitic stainless steels at cryogenic temperatures. Cryogenics, 40, 251-259

[14]. Norman, A. F., Drazhner, V., & Prangnell, P. B. (1999). Effect of welding parameters on the solidification microstructure of autogenous TIG welds in an Al– Cu–Mg–Mn alloy. Materials Science and Engineering: A, 259(1), 53-64.

[15]. Song, J. L., Lin, S. B., Yang, C. L., & Fan, C. L. (2009). Effects of Si additions on intermetallic compound layer of aluminum–steel TIG welding–brazing joint. Journal of Alloys and Compounds, 488(1), 217-222.

[16]. Wang, Q., Sun, D. L., Na, Y., Zhou, Y., Han, X. L., & Wang, J. (2011). Effects of TIG Welding Parameters on Morphology and Mechanical Properties of Welded Joint of Ni-base Superalloy. Procedia Engineering, 10, 37-41.